DR. XUHUI WANG (Orcid ID : 0000-0003-0818-9816)

DR. SHILONG PIAO (Orcid ID : 0000-0001-8057-2292)

DR. CHRIS HUNTINGFORD (Orcid ID : 0000-0002-5941-7770)

DR. ANA BASTOS (Orcid ID : 0000-0002-7368-7806)

DR. ANPING CHEN (Orcid ID : 0000-0003-2085-3863)

Unusual characteristics of the carbon cycle during the 2015−2016 El Niño

Running Title: Unusual carbon cycle in the 2015−2016 El Niño

Kai Wang[1], Xuhui Wang[1], Shilong Piao[1,2,3], Frédéric Chevallier[4], Jiafu Mao[5], Xiaoying Shi[5], Chris Huntingford[6], Ana Bastos[7], Philippe Ciais[4], Hao Xu[1], Ralph F. Keeling[8], Stephen W. Pacala[9], Anping Chen[10*]

[1]Sino-French Institute for Earth System Science, College of Urban and Environmental Sciences, Peking University, Beijing, China

[2]Key Laboratory of Alpine Ecology and Biodiversity, Institute of Tibetan Plateau Research, Chinese Academy of Sciences, Beijing, China

[3]Center for Excellence in Tibetan Earth Science, Chinese Academy of Sciences, Beijing, China

[4]Laboratoire des Sciences du Climat et de l'Environnement, CEA CNRS UVSQ, Gif-sur-Yvette, France

[5]Environmental Sciences Division, Oak Ridge National Laboratory, Oak Ridge, TN, USA

[6]UK Center for Ecology and Hydrology, Wallingford, UK

[7]Department Biogeochemical Integration, Max Planck Institute for Biogeochemistry, Jena,

This article has been accepted for publication and undergone full peer review but has not been through the copyediting, typesetting, pagination and proofreading process, which may lead to differences between this version and the Version of Record. Please cite this article as doi: 10.1111/GCB.15669

Germany

[8]Scripps Institution of Oceanography, University of California, San Diego, La Jolla, California, USA

[9]Department of Ecology and Evolutionary Biology, Princeton University, Princeton, USA

[10]Department of Biology and Graduate Degree Program in Ecology, Colorado State University, Fort Collins, USA

* Corresponding author. Email: anping.chen@colostate.edu

Abstract

The 2015−2016 El Niño was one of the strongest on record, but its influence on the carbon balance is less clear. Using Northern Hemisphere atmospheric CO_2 observations, we found both detrended atmospheric CO_2 growth rate (CGR) and CO_2 seasonal-cycle amplitude (SCA) of 2015−2016 were much higher than that of other El Niño events. The simultaneous high CGR and SCA were unusual, because our analysis of long-term CO_2 observations at Mauna Loa revealed a significantly negative correlation between CGR and SCA. Atmospheric inversions and terrestrial ecosystem models indicate strong northern land carbon uptake during spring but substantially reduced carbon uptake (or high emissions) during early autumn, which amplified SCA but also resulted in a small anomaly in annual carbon uptake of northern ecosystems in 2015−2016. This negative ecosystem carbon uptake anomaly in early autumn was primarily due to soil water deficits and more litter decomposition caused by enhanced spring productivity. Our study demonstrates a decoupling between seasonality and annual carbon cycle balance in northern ecosystems over 2015−2016, which is unprecedented in the past five decades of El Niño events.

KEYWORDS

CO_2 seasonal-cycle amplitude (SCA), atmospheric CO_2 growth rate (CGR), El Niño, net biome productivity (NBP), northern terrestrial ecosystems, soil water deficit

1 | INTRODUCTION

The El Niño-Southern Oscillation (ENSO) is a quasi-periodic sea surface temperature variation of the central to eastern Pacific Ocean, with prominent impacts on Earth's surface climate system (McPhaden et al., 2006; Timmermann et al., 2018). The extreme phases of the ENSO cycle can induce extreme weather events, which in turn affect the structure and function of ecosystems worldwide (McPhaden et al., 2006; Piao et al., 2020). For example, the observed fluctuation of atmospheric CO_2 growth rate (CGR) is found to be tightly correlated with the ENSO cycle (Wang et al., 2013). Yet the CGR variation is strongly influenced by annual variations in land-atmosphere fluxes, rather than by ocean or anthropogenic emissions (Jeong et al., 2018; Le Quéré et al., 2018; Piao et al., 2020). Hence this close relationship between CGR and ENSO implies an important role of the ENSO cycle in terrestrial ecosystem carbon cycle. Considering that many climate model simulations project increases in the frequency of extreme ENSO events, and intensified sensitivity of land carbon cycle to ENSO with background global warming (Kim et al., 2017; Wang et al., 2019), there is an urgent need to better understand the terrestrial ecosystem response to ENSO to refine projections of the carbon cycle in the future.

The latest extreme El Niño event in 2015−2016 was one of the strongest on record (Santoso et al., 2017). These two years also exhibited the two largest CGR of the last fifty years from CO_2 mole fraction data (Dlugokencky & Tans, 2020). Due to the large CGR, the year of 2016 was iconic as the first full year in which every monthly mean CO_2 mole fraction remained above 400 ppm all year round. This is the first such all year occurrence of crossing this threshold since the beginning of human observations of atmospheric CO_2 (Dlugokencky & Tans, 2020; Scripps Institution of Oceanography, 2020). The large CGR reflects a weakened land carbon sink in both years 2015 and 2016 (Bastos et al., 2018) and thus has attracted vast interest (Hu et al., 2019; Liu et al., 2017; Wang et al., 2018; Yue et al., 2017). For example, the U.K. Royal Society published a special issue of 22 papers discussing the impact of the 2015−2016 El Niño event on the tropical carbon cycle in the journal *Philosophical Transactions of the Royal Society B* (Malhi et al., 2018). However, it is much less noted that these two years also witnessed the highest CO_2 seasonal-cycle amplitude (SCA, the peak-to-trough magnitude of the detrended season cycle of CO_2; see Section 2.7) of the past four decades at the Mauna Loa Observatory (MLO) station (Figure 1a). At first glance, the co-emergence of both the highest CGR and highest SCA in the 2015−2016 El Niño is surprising because a high SCA value implies a strong carbon uptake during the net carbon uptake

period (CUP) (see Section 2.8), in contrast to high CGR-indicated carbon sink weakening. In fact, historical data since 1980 show a significant negative correlation between CGR and SCA in the MLO record when excluding 2015−2016 (R^2 = 0.52, P = 0.03; Figure 1a). Therefore, the primary objective of this study is to resolve this apparent paradox.

Here, we utilized atmospheric CO_2 records from the surface observation network (Dlugokencky et al., 2018), satellite observations of solar-induced fluorescence (SIF) (Joiner et al., 2013) and Normalized Difference Vegetation Index (NDVI) (Pinzon & Tucker, 2014), net land-atmosphere CO_2 fluxes from atmospheric inversions based on surface in situ stations (Chevallier et al., 2005; Rödenbeck et al., 2003), and column CO_2 mole fraction (X_{co2}) retrievals from the Orbiting Carbon Observatory-2 (OCO-2) (Chevallier et al., 2019). To provide process understanding support, we additionally employed the ensemble of Dynamic Global Vegetation Models (DGVMs) from TRENDYv6 (Le Quéré et al., 2018; Sitch et al., 2015). This combined data and simulation framework allowed us to investigate the mechanisms behind the observed unusual signals of CGR and SCA during the 2015−2016 El Niño.

2 | MATERIALS AND METHODS

2.1 | Atmospheric CO_2 mole fraction data

We used monthly CO_2 mole fraction data, collected at the MLO site, for years 1958−2018 from the Earth System Research Laboratory (ESRL), National Oceanic and Atmospheric Administration (NOAA) (www.esrl.noaa.gov/gmd/ccgg/trends/). Note the NOAA ESRL CO_2 data from March in 1958 through April in 1974 was obtained from the Scripps Institution of Oceanography (https://scrippsco2.ucsd.edu/). We also used monthly CO_2 mole fraction data from the NOAA ESRL Carbon Cycle Cooperative Global Air Sampling Network (Dlugokencky et al., 2018), which is available for many locations around the world. For a credible comparison between an El Niño composite (the spatial average of El Niño events) and 2015−2016 El Niño, we selected 32 sites with at least 20 years of data covering 2015−2016.

2.2 | Climate dataset

Monthly gridded air temperature and precipitation data for 1980 to 2016 were obtained from the Climatic Research Unit (CRU TS4.01) with a spatial resolution of 0.5° (Harris et al., 2014). We

also used the shortwave radiation data obtained from the 6-hourly reanalysis dataset CRU-NCEPv8 with a spatial resolution of 0.5°, which is based on monthly CRU climate data. The CRU-NCEPv8 climate dataset is also the forcing data set of DGVMs in the TRENDYv6 project (Le Quéré et al., 2018).

2.3 | NDVI and SIF data

The third generation data of Normalized Difference Vegetation Index (NDVI3g) from the Global Inventory Monitoring and Modelling Studies (GIMMS) group was used in this study to represent vegetation greenness (Pinzon & Tucker, 2014). The GIMMS NDVI3g provides a global NDVI product, at 15-day temporal resolution and 8-km spatial resolution for 1982−2016. We remapped the gridded NDVI values to match the 0.5° grid.

SIF is an electromagnetic signal emitted by chlorophyll during photosynthesis and is thus expected to give a direct assessment of actual photosynthesis (Chen et al., 2021; Joiner et al., 2013). We used a SIF product derived from data acquired by the Global Ozone Monitoring Experiment-2 (GOME-2) spectrometer on board EUMETSAT's polar orbiting Meteorological Operational Satellites-A (MetOp-A) (Joiner et al., 2013). The monthly SIF data are available at 0.5° spatial resolution for 2007−2017. Hence both NDVI and SIF data cover our 2015−2016 period of interest.

2.4 | Atmospheric CO_2 inversion fluxes

We used the posteriori estimated land surface CO_2 fluxes derived from two long-term atmospheric in situ inversions covering 1980−2016: Copernicus Atmosphere Monitoring Service (CAMS, http://atmosphere.copernicus.eu/) version 17r1 and Jena CarboScope (Jena) version s76_v4.2. The two atmospheric inversions are both based on in situ CO_2 measurements from monitoring stations. CAMS version 17r1 provides monthly fluxes at 1.9°latitude×3.75°longitude resolution for 1979−2017 and Jena CarboScope version s76_v4.2 provides monthly fluxes at 4°latitude×5°longitude resolution for 1976−2017 (Chevallier et al., 2005; Rödenbeck et al., 2003). We mainly used remapped output of land CO_2 fluxes with a spatial resolution of 1°. To obtain the net biome productivity (NBP) anomaly in latitudinal bins of 5°, the gridded CO_2 fluxes were also remapped to match the 5° grid. Since we focus on the impact of 2015−2016 extreme climatic conditions on carbon cycle, the long-term trend of NBP anomaly in each month was removed.

We also used another version of CAMS inversion (CAMS vFT18r1) that assimilates X_{CO2} retrievals (Chevallier et al., 2019). The satellite-retrieved X_{CO2} retrievals were from NASA's OCO-2 v9, and available for late-2014 to 2018 (Eldering et al., 2017). To invert for surface CO_2 fluxes from X_{CO2} retrievals, the Laboratoire de Météorologie Dynamique (LMDZ) atmospheric transport model was used (Chevallier et al., 2005). The LMDZ transport model was run on a 1.9º×3.75º (latitude × longitude) horizontal grid, with 39 layers between the surface and the top of the atmosphere. LMDZ was nudged to European Centre for Medium-Range Weather Forecasts (ECMWF) analyzed winds. The anomaly of land surface CO_2 flux in 2015−2016, as estimated by this inversion, is relative to land surface CO_2 flux in 2018 because observation-based CGR and SCA in 2018 are closer to the long-term averages during 1980−2018 than those in 2017. In this study, for simplicity, we refer to these two strands of data of CAMS vFT18r1 by "$CAMS_{OCO-2}$" and of CAMS v17r1 by "CAMS".

2.5 | Dynamic Global Vegetation Models

We analyzed the monthly anomalies of NBP, gross primary productivity (GPP), autotrophic respiration (Ra) and heterotrophic respiration (Rh) for years 1980−2016, as estimated by an ensemble of twelve Dynamic Global Vegetation Models (DGVMs) from the TRENDYv6 project (Le Quéré et al., 2018; Sitch et al., 2015). DGVMs used in this study are CABLE, CLASS-CTEM, CLM4.5, ISAM, JSBACH, JULES, LPJ, LPX, ORCHIDEE, ORCHIDEE-MICT, VEGAS and VISIT. All models in the "S3" simulations of the TRENDYv6 protocol were forced by the same data including a climate dataset obtained from CRU-NCEPv8, atmospheric CO_2 mole fraction data from a combination of ice core records and atmospheric observations, and land use change data from the HYDE data set. We also analyzed the simulated carbon flux from vegetation to litter pool (fVegLitter) and from litter pool to soil (fLitterSoil), although only two models of ORCHIDEE and ORCHIDEE-MICT have output these two quantities. We calculated anomalies in these carbon fluxes (NBP, GPP, Ra, Rh, fVegLitter and fLitterSoil), for each month, by removing the long-term trend of carbon fluxes of each month.

2.6 | El Niño events

We selected the El Niño events following NOAA's criteria of the Ocean Niño Index (ONI) (https://origin.cpc.ncep.noaa.gov/). The ONI is a 3-month running mean of sea surface temperature anomalies (SSTA) averaged in the Niño 3.4 region (5°N–5°S, 120°–170°W). The El

Niño events are defined based on the ONI criteria that the ONI be greater than or equal to +0.5 °C for a period of at least five consecutive overlapping 3-month seasons. The El Niño events since 1959 that fulfill that criteria, and that we used in this study, occur in 1963−1964, 1965−1966, 1968−1969, 1972−1973, 1976−1977, 1979−1980, 1982−1983, 1987−1988, 1991−1992, 1994−1995, 1997−1998, 2002−2003, 2004−2005, 2006−2007, 2009−2010 and 2015−2016.

2.7 | Derivation of the CGR and SCA

Annual CGR, for any particular year, were calculated by subtracting the four-month average of CO_2 mole fraction centered on the January 1 of this year from the four-month average centered on the January 1 of the next year. The long-term trend of CGR was mainly induced by carbon emissions from fossil fuel burning and was removed using linear regression to obtain the CGR anomalies.

The SCA was extracted using the tool CCGCRV (Thoning et al., 1989). CCGCRV approximated the long-term growth and annual oscillation using a function consisting of a quadratic polynomial and four-harmonics, all fitted to the CO_2 mole fraction data. The seasonal harmonics did not include any short-term variations, so a 50-day cutoff value short term filter was applied to the residuals derived between the raw data and fitted function. Finally, the smoothed CO_2 seasonal cycle was obtained by adding the filtered residuals to the annual oscillation. The peak-to-trough amplitude was calculated as the difference between the maximum and the minimum CO_2 mole fraction of the seasonal cycle in each calendar year (Wang et al., 2020). Since there are one CGR value and one SCA value every year, the CGR or SCA of 2015−2016 indicates the average of that in 2015 and 2016.

2.8 | Net carbon uptake period

SCAs from most temperate and boreal stations of the Northern Hemisphere generally reflect the net carbon uptake during April−August (Piao et al., 2018). Therefore, the CUP used in this study corresponds to that period of April−August for each year. It should be noted that NBP during August in some regions could have little influence in the magnitude of peak-to-trough of CO_2 concentration. However, it could influence the magnitude of trough-to-peak concentrations in some remote stations, likely due to atmospheric CO_2 transport.

3 | RESULTS

3.1 | Ubiquitous and unusual high SCA during the 2015−2016 El Niño

We first verified that the unusual SCA signal in 2015−2016 at MLO was not an artifact of averaging the two years – separate analyses of the CO_2 mole fraction data in 2015 and 2016 also confirmed this finding (Figure 1a; Figure S1). Furthermore, the SCA in 2015−2016 was also the highest on record when extending the analysis back to 1959, the first year with a year-complete CO_2 record at MLO (Figure S1). We also confirmed the unusually high SCA in 2015−2016 by analyzing CO_2 mole fraction data from an atmospheric observation network of 32 long-term sites in the Northern Hemisphere (each site with at least 20 years of data covering 2015−2016). We found that the SCA in 2015−2016 was significantly larger by 0.52±0.14 ppm (mean±SE) than that of the long-term average during El Niño events ($P < 0.01$; Figure 1b).

3.2 | Tropical versus extra-tropical northern lands in their contributions to the high CGR and SCA in 2015−2016

Next, we analyzed the NBP anomalies of both northern (north of 30°N) and tropical ecosystems from the two long-term in situ inversions (CAMS and Jena CarboScope) and for each El Niño event since 1980. We found that although there was a significant positive correlation between SCA and annual NBP of northern ecosystems during El Niño events in the recent three decades excluding 2015−2016 ($R^2 = 0.86$, $P < 0.01$), the annual NBP anomaly of northern ecosystems (−0.18 to 0.21 PgC yr^{-1}) in 2015−2016 was within the range of the average during El Niño events since 1980 (−0.05±0.28 PgC yr^{-1}; uncertainty range is the standard deviation (SD) of NBP anomalies in El Niño events, derived from the two inversions; Figure 1c and Table S1). The comparable annual NBP of northern ecosystems in 2015−2016 with that in other El Niño events contributed little to the anomalies of global NBP in this recent El Niño event and thus did not affect the dominant role of tropical ecosystems in controlling the variation of CGR (Figure 1c, d). We found that the relationship between tropical annual NBP and CGR across El Niño events did not change with or without the inclusion of the 2015−2016 El Niño (Figure 1d).

With these two in situ inversions, we further compared net carbon exchange during CUP and non-CUP in northern ecosystems and tropical lands for different El Niño events. We found that in northern ecosystems, the difference between CUP and non-CUP net carbon exchange had a large

increase in 2015−2016 when compared to the average during the El Niño events since 1980 (10 events in total) (Table S1). By contrast, results from CAMS inversion showed that the increase of the net carbon exchange difference between CUP and non-CUP from tropical ecosystems in 2015−2016, when compared with the average of El Niño events, was smaller than that in northern ecosystems. Furthermore, the Jena CarboScope inversion showed that in tropical ecosystems, there was no significant difference in CUP minus non-CUP net carbon exchange between 2015−2016 and the average of El Niño events. Critically, we also found that the net land carbon uptake in northern extra-tropics during the 2015−2016 CUPs was significantly larger than that of the average during all the El Niño events since 1980 (Table S1). In contrast, net carbon uptake by tropical lands during the 2015−2016 CUPs, derived from the atmospheric CO_2 measurements, did not increase when compared to its average behavior during El Niño years (Table S1). Therefore, the unusually high SCA of 2015−2016 was mainly contributed by northern ecosystems.

3.3 | Northern ecosystem NBP anomalies in April−June and August−September

Both atmospheric in situ inversions and additional DGVMs showed that compared to other El Niño events, the relatively high NBP of northern ecosystems during the 2015−2016 El Niño mainly appeared during the April−June part of CUP (Figure 2; Figures S2 and S3). The net biosphere CO_2 flux estimation inferred from the OCO-2 inversion ($CAMS_{OCO\text{-}2}$) also showed high NBP during April−June of 2015−2016 (Figure 3a). In addition, the NBP anomaly of northern ecosystems during April−June was significantly related to SCA for other El Niño events, during 1980−2016 ($P \leq 0.01$; Figure S3). However, the strengthened spring net carbon sink was largely offset by strong negative NBP anomalies from August to September, resulting in comparable annual NBP of northern ecosystems in 2015−2016 with that in other El Niño events (Figure 2). $CAMS_{OCO\text{-}2}$ and two in situ inversions also showed that seasonal NBP anomalies in regions having larger-than-normal spring NBP could largely explain the seasonality of northern extra-tropical NBP anomaly in 2015−2016 (Figure 2; Figure S4).

Figure 3 shows the spatial distribution of NBP anomalies during April−June and August−September of 2015−2016. Results from the $CAMS_{OCO\text{-}2}$ inversion, in situ inversions (CAMS and Jena CarboScope) and the DGVMs agreed on high positive NBP anomalies in western North America and southern West Siberia during April−June of 2015−2016 (Figure 3). In addition, large positive NBP anomalies of these two regions were confirmed independently, as

found to be associated with enhanced photosynthesis (Figure 4). This enhanced photosynthesis was supported by positive anomalies of satellite observed vegetation greenness (NDVI) data, in April−June for both 2015 and 2016 years (Figure 4a). In particular for these years, the April−June NDVI value positively departed from their long-term average by 1.70 and 1.38 SD in western North America and southern West Siberia, respectively. Results from analyses of SIF data also showed enhanced photosynthesis in those two regions during this recent period (Figure 4c). In the next section, we provide a detailed analysis on seasonal NBP anomalies of the regions in northern extra-tropics.

3.4 | Seasonal NBP anomalies in western North America and western Russia

In western North America, an El Niño event is generally featured with high spring temperature (Figure S5). Indeed, historical climate data showed that in this region, the temperature of April−June in the extreme 2015−2016 El Niño event was much higher than the average of El Niño events since the 1980s for the same months (Figures S5 and S6). Similarly, high temperatures were also observed in northern West Siberia during April−June for both 2015 and 2016 (Figures S5 and S6). For northern West Siberia, $CAMS_{OCO\text{-}2}$ inversion, Jena CarboScope and DGVMs all showed more net carbon uptake during April−June of 2015−2016 as a result of high vegetation productivity (Figures 3 and 4). In contrast, low temperature occurred in northeastern North America and eastern Siberia (Figure S6), where we found negative anomalies of satellite NDVI and SIF during April−June for both 2015 and 2016 (Figure 4a, c). This negative vegetation productivity anomaly induced by low temperature was also captured by most DGVMs (Figure 4e). In addition, precipitation may also contribute to the positive NBP anomalies in southern West Siberia. In this region, both satellite data and DGVMs showed high vegetation productivity during April−June in 2015−2016, corresponding to higher-than-average precipitation for this location, where temperature was within the normal range and solar radiation was lower than the normal conditions during this same period (Figures 4; Figures S5 and S6).

Although there was a relative high spring NBP in western North America, no strong carbon uptake was found during August−September of 2015−2016 by the $CAMS_{OCO\text{-}2}$, in situ inversions and DGVMs (Figure 3). Instead, we found large negative NBP anomalies for those particular months, based on inversions using OCO-2 X_{co2} retrievals and in situ data (Figure 3). Similarly, satellite data also revealed lower-than-normal NDVI and SIF values during August−September of

2015−2016 for western North America, and despite high positive spring NDVI and SIF anomalies of the two years (Figures 4 and 5). This reduced productivity is of particular interest, as temperature, precipitation and shortwave radiation during August−September of 2015−2016 were all comparable to the long-term averages of early autumn from 1980 to 2016 (Figure 5; Figure S6). Furthermore, most DGVMs failed to capture the significant decrease of vegetation productivity observed in NDVI and SIF records, which explains their underestimation of negative NBP anomalies during August−September of 2015−2016 (Figure 4f; Figure S4).

In western Russia, as for western North America, high negative NDVI and SIF anomalies in the early autumn of 2015−2016 were also found (Figure 4b, d). However, these were instead likely caused by the reduction of solar radiation due to the increase of rainfall-associated clouds (Figure S6). Climate data showed higher-than-average precipitation and lower-than-average solar radiation occurred in this region during September of 2015−2016 (Figure S6). This largely reduced land carbon uptake during August−September of 2015−2016 in western Russia was also reproduced by both inversions based on OCO-2 X_{co2} retrievals and in situ inversions (Figure 3), but not by most DGVMs (Figure 3h; Figure S7).

Process-based models showed that in regions with higher spring NBP in 2015−2016 than normal years, there was also more litter in the autumn (Figure S8). In western North America, low temperatures in September of both 2015 and 2016 suppressed the litter decomposition and thus the heterotrophic respiration (Figure 5). By contrast, high temperatures in western Russia during the same period accelerated the decomposition of litter and contributed to the negative NBP anomalies in early autumns (Figure 5), which could also increase the SCA. As an additional sensitivity study, analyses of fire emissions show that fires have limited impacts on the seasonal NBP anomalies of northern ecosystems in 2015−2016 (Figure S9).

4 | DISCUSSION

In El Niño years, when the atmospheric CGR anomaly is highly enhanced, the SCA is generally largely reduced. However, by examining CO_2 monitoring data from the Mauna Loa Observatory and other observation sites, we found co-occurring high CGR and SCA during the 2015−2016 El Niño, breaking the otherwise negative correlation between CGR and SCA over the last five

decades' El Niño events. We showed that while tropical lands dominated CGR variations, the unusually high SCA of 2015−2016 was mainly caused by increased NBP during CUP in northern ecosystems. Previous research has also demonstrated that enhanced northern ecosystem vegetation activity is responsible for the increase of SCA (Forkel et al., 2016; Graven et al., 2013; Wang et al., 2020). However, it was unclear why this enhanced northern ecosystem growth did not lead to more ecosystem carbon uptake (i.e., reduced CGR).

There are two mutually exclusive hypotheses (H1 and H2) to explain the unusual concurrence of high SCA and CGR in the 2015−2016 El Niño. These hypotheses are: (H1) higher northern land carbon uptake during CUP induced a high annual net land sink of northern ecosystems in 2015−2016, which was offset by annually reduced carbon uptake or even carbon emissions from tropical ecosystems; (H2) higher northern land carbon uptake during CUP did not induce overall high annual net land carbon sink of northern ecosystems in 2015−2016, compared to the average of El Niño events since 1980. Under Hypothesis (H2), high northern land carbon emissions during off-seasons would offset its growing season land carbon sequestrations, and so overall the reduced tropical uptake accounted for most of the CGR anomaly. Our result indicated that the higher land net carbon uptake during CUPs of 2015−2016 did not lead to a higher annual net land sink in northern ecosystems compared to other El Niño events (Figure 1c). This finding, therefore, supported Hypothesis (H2) and allowed the rejection of Hypothesis (H1). Moreover, the tropics-based finding gave additional evidence supporting Hypothesis (H2) (Figure 1d).

The high SCA in 2015−2016 is mainly contributed by the increased carbon uptake of northern ecosystems during April−June. Moreover, the significantly positive correlation between NBP anomaly of northern ecosystems during April−June and SCA also underlines the role of NBP anomaly during April−June in regulating the variations of SCA. This result is consistent with previous findings, that enhanced SCA could be explained by the increase of carbon uptake in the early growing season (Angert et al., 2005; Randerson et al., 1999). It has been suggested that higher air temperature is the dominant climatic driver in the increased spring vegetation productivity (Chen et al., 2018). For example, higher spring vegetation productivity in western North America and northern West Siberia was likely driven by the relative high spring temperature, which is known to advance the start of the growing season (Dannenberg et al., 2015; Keenan et al., 2014; Randerson et al., 1999). Although we also found both high productivity and

strong solar radiation in western North America and northern West Siberia during April−June of 2015−2016 (Figures 3 and 4; Figures S5 and S6), the impacts of solar radiation to spring vegetation productivity are suggested to be much weaker than temperature (Chen et al., 2018).

It has been frequently suggested that the strong net carbon uptake of North America in spring is significantly influenced by El Niño-associated higher temperatures (Figure S5) (Buermann et al., 2003; Dannenberg et al., 2015; Hu et al., 2019). However, this may not present a complete representation of the overall response of annual carbon uptake in northern ecosystems to El Niño. By focusing on the unusual 2015−2016 El Niño, we show that higher productivity in spring does not always enhance the annual carbon sink due to seasonal compensation of NBP anomalies in northern ecosystems. For example, although previous studies suggested that El Niño events enhance annual net carbon uptake in North America, and specifically in western North America (Hu et al., 2019), annual net carbon uptake in western North America during 2015−2016 was lower than its long-term average. With the two in situ inversions, we estimated that the annual uptake was reduced by 13%−25% compared to the average of annual uptake in 1980−2016, caused by the large offset by negative NBP anomalies in the early autumns. The findings in the early autumn, and for North America and Russian regions, in particular, provide empirical support of Hypothesis (H2).

The offset of spring positive NBP anomalies by early autumn negative NBP anomalies found in 2015−2016 could not solely result from the El Niño-associated anomalies of climatic drivers in two seasons, although such anomalies could largely regulate the anomalies of autumn NBP when the strength of El Niño events is either weak or moderate. For example, the large negative NBP anomalies during August−September of 2015−2016 are mainly located in western North America and western Russia, but the mechanisms for explaining this seasonal compensation of NBP are found to be different between these two regions. We propose that the lower vegetation productivity in western North America during early autumn of 2015−2016 was caused by soil water deficits, themselves driven by lack of water supply in June and enhanced evapotranspiration from higher spring vegetation productivity (Figures 5 and 6) (Buermann et al., 2013, 2018; Lian et al., 2020). In addition, more litter in the autumn of 2015−2016 than normal years is found in regions with higher spring vegetation productivity. This indicates that besides weakened productivity, the observed negative NBP anomalies in early autumns of 2015−2016 could also be

attributed to increased carbon respiration loss. Higher productivity in spring will have increased fast-cycling leaf carbon allocation, resulting in enhanced autumnal litter pool (Figure 6), but such litter also tends to decompose fast. Our study thus emphasizes the need to understand both the effect of enhanced vegetation productivity in spring, any autumn offsets of this, their inter-connections and links to seasonal climatic anomalies triggered by El Niño events (Buermann et al., 2003; Yue et al., 2017). Such understanding will support a better assessment of the northern ecosystem carbon cycle to extreme El Niño events, and in the context of background climate change (Hu et al., 2019). In 2015−2016, spring temperature in western North America and western Russia are much higher than that of other El Niño events, resulting in anomalously high productivity. The spring productivity in 2015−2016 thus has larger impacts on autumn NBP than previous El Niño events, by high productivity induced soil water deficit and more litter decomposition (Buermann et al., 2018; Lian et al., 2020).

The frequency of extreme El Niño events is likely to increase under future climate change (Wang et al., 2019). The significant negative correlation between SCA and CGR during previous El Niño events excluding 2015−2016 event underlines the contribution of northern extra-tropical carbon balance during CUP to the variation of global land carbon budget during those periods (Figure 1a; Figure S1). Furthermore, analysis of our finding of the unusual carbon cycle patterns during the 2015−2016 El Niño event, and especially its changed seasonal variation, also implies that the northern extra-tropics cannot be neglected in any understanding of the impacts of extreme El Niño events on the global carbon cycle. Currently, it is unclear whether the 2015−2016 carbon cycle change, especially in northern ecosystems, during the extreme El Nino event is a special case, or will become a new norm under strong El Niño events in the future and as atmospheric greenhouse gases rise (McPhaden et al., 2006; Timmermann et al., 2018).

The spatial patterns of carbon uptake during early autumn periods revealed from in situ and satellite-based inversions could not be fully reproduced by state-of-the-art DGVMs. We suggest this is because drivers controlling ecosystem carbon dynamics in autumn are more complex and co-vary with any legacy of previous seasons (Buermann et al., 2018; Keenan et al., 2014; Lian et al., 2020; Zhang et al., 2020). For example, early autumn vegetation productivity in western Russia is more limited by radiation, rather than by temperature or precipitation (Chen et al., 2018; Zhang et al., 2020). In addition, most state-of-the-art DGVMs likely overestimate the sensitivity of

ecosystem carbon uptake to precipitation (Mystakidis et al., 2017), which could incorrectly compensate the impacts of low solar radiation levels. To reduce uncertainties in simulating the spatiotemporal pattern of carbon uptake by DGVMs, and especially for autumn periods, a priority would be to improve model representation of key terrestrial ecosystem processes through integrating atmospheric observation and field experiments.

In summary, our analysis based on atmospheric CO_2 observation, atmospheric inversions and process-based models revealed the seasonal characteristic of carbon cycle in northern ecosystems during 2015−2016 El Niño event, which is unusual compared with previous El Niño events. This study provides a new paradigm and methodological approach to evaluate potential interactions of the atmosphere-hydrosphere-biosphere system in northern extra-tropics during strong El Niño events. Unlike other studies, our emphasis has been to understand more fully a single extreme El Niño event and the corresponding dynamics of terrestrial carbon cycle. Our approach raises confidence in the ability to explain anomalous climate-carbon cycle events. This knowledge may be critical should rare events become more frequent as both the climate and global carbon cycle systems evolve in response to anthropogenic forcing.

REFERENCES

Angert, A., Biraud, S., Bonfils, C., Henning, C. C., Buermann, W., Pinzon, J., Tucker, C. J., & Fung, I. (2005). Drier summers cancel out the CO_2 uptake enhancement induced by warmer springs. *Proceedings of the National Academy of Sciences*, *102*(31), 10823–10827. https://doi.org/10.1073/pnas.0501647102

Bastos, A., Friedlingstein, P., Sitch, S., Chen, C., Mialon, A., Wigneron, J.-P., Arora, V. K., Briggs, P. R., Canadell, J. G., Ciais, P., Chevallier, F., Cheng, L., Delire, C., Haverd, V., Jain, A. K., Joos, F., Kato, E., Lienert, S., Lombardozzi, D., … Zhu, D. (2018). Impact of the 2015/2016 El Niño on the terrestrial carbon cycle constrained by bottom-up and top-down approaches. *Philosophical Transactions of the Royal Society B: Biological Sciences*, *373*(1760), 20170304. https://doi.org/10.1098/rstb.2017.0304

Buermann, W., Anderson, B., Tucker, C. J., Dickinson, R. E., Lucht, W., Potter, C. S., & Myneni, R. B. (2003). Interannual covariability in Northern Hemisphere air temperatures and

greenness associated with El Niño-Southern Oscillation and the Arctic Oscillation. *Journal of Geophysical Research: Atmospheres*, *108*(D13), 4396. https://doi.org/10.1029/2002JD002630

Buermann, W., Bikash, P. R., Jung, M., Burn, D. H., & Reichstein, M. (2013). Earlier springs decrease peak summer productivity in North American boreal forests. *Environmental Research Letters*, *8*(2). https://doi.org/10.1088/1748-9326/8/2/024027

Buermann, W., Forkel, M., O'Sullivan, M., Sitch, S., Friedlingstein, P., Haverd, V., Jain, A. K., Kato, E., Kautz, M., Lienert, S., Lombardozzi, D., Nabel, J. E. M. S., Tian, H., Wiltshire, A. J., Zhu, D., Smith, W. K., & Richardson, A. D. (2018). Widespread seasonal compensation effects of spring warming on northern plant productivity. *Nature*, *562*(7725), 110–114. https://doi.org/10.1038/s41586-018-0555-7

Chen, A., Mao, J., Ricciuto, D., Xiao, J., Frankenberg, C., Li, X., Thornton, P. E., Gu, L., & Knapp, A. K. (2021). Moisture availability mediates the relationship between terrestrial gross primary production and solar-induced chlorophyll fluorescence: Insights from global-scale variations. *Global Change Biology*, *27*(6), 1144–1156. https://doi.org/10.1111/gcb.15373

Chen, C., He, B., Guo, L., Zhang, Y., Xie, X., & Chen, Z. (2018). Identifying Critical Climate Periods for Vegetation Growth in the Northern Hemisphere. *Journal of Geophysical Research: Biogeosciences*, *123*(8), 2541–2552. https://doi.org/10.1029/2018JG004443

Chevallier, F., Fisher, M., Peylin, P., Serrar, S., Bousquet, P., Bréon, F.-M., Chédin, A., & Ciais, P. (2005). Inferring CO_2 sources and sinks from satellite observations: Method and application to TOVS data. *Journal of Geophysical Research*, *110*(D24), D24309. https://doi.org/10.1029/2005JD006390

Chevallier, F., Remaud, M., O'Dell, C. W., Baker, D., Peylin, P., & Cozic, A. (2019). Objective evaluation of surface- and satellite-driven carbon dioxide atmospheric inversions. *Atmospheric Chemistry and Physics*, *19*(22), 14233–14251. https://doi.org/10.5194/acp-19-14233-2019

Dannenberg, M. P., Song, C., Hwang, T., & Wise, E. K. (2015). Empirical evidence of El Niño-Southern Oscillation influence on land surface phenology and productivity in the

western United States. *Remote Sensing of Environment*, *159*, 167–180. https://doi.org/10.1016/j.rse.2014.11.026

Dlugokencky, E. J., Lang, P. M., Mund, J. W., Crotwell, A. M., Crotwell, M. J., & Thoning, K. W. (2018). *Atmospheric Carbon Dioxide Dry Air Mole Fractions from the NOAA ESRL Carbon Cycle Cooperative Global Air Sampling Network, 1968-2017, Version: 2018-07-31*. Available at: Path: Ftp://Aftp.Cmdl.Noaa.Gov/Data/Trace_gases/Co2/Flask/Surface.

Dlugokencky, E., & Tans, P. (2020). *Trends in atmospheric carbon dioxide*. National Oceanic & Atmospheric Administration; Earth System Research Laboratory (NOAA/ESRL). https://www.esrl.noaa.gov/gmd/ccgg/trends/

Eldering, A., Wennberg, P. O., Crisp, D., Schimel, D. S., Gunson, M. R., Chatterjee, A., Liu, J., Schwandner, F. M., Sun, Y., O'Dell, C. W., Frankenberg, C., Taylor, T., Fisher, B., Osterman, G. B., Wunch, D., Hakkarainen, J., Tamminen, J., & Weir, B. (2017). The Orbiting Carbon Observatory-2 early science investigations of regional carbon dioxide fluxes. *Science*, *358*(6360), eaam5745. https://doi.org/10.1126/science.aam5745

Forkel, M., Carvalhais, N., Rödenbeck, C., Keeling, R., Heimann, M., Thonicke, K., Zaehle, S., & Reichstein, M. (2016). Enhanced seasonal CO_2 exchange caused by amplified plant productivity in northern ecosystems. *Science*, *351*(6274), 696–699. https://doi.org/10.1126/science.aac4971

Graven, H. D., Keeling, R. F., Piper, S. C., Patra, P. K., Stephens, B. B., Wofsy, S. C., Welp, L. R., Sweeney, C., Tans, P. P., Kelley, J. J., Daube, B. C., Kort, E. A., Santoni, G. W., & Bent, J. D. (2013). Enhanced seasonal exchange of CO_2 by Northern ecosystems since 1960. *Science*, *341*(6150), 1085–1089. https://doi.org/10.1126/science.1239207

Harris, I., Jones, P. D., Osborn, T. J., & Lister, D. H. (2014). Updated high-resolution grids of monthly climatic observations - the CRU TS3.10 Dataset. *International Journal of Climatology*, *34*(3), 623–642. https://doi.org/10.1002/joc.3711

Hu, L., Andrews, A. E., Thoning, K. W., Sweeney, C., Miller, J. B., Michalak, A. M., Dlugokencky, E., Tans, P. P., Shiga, Y. P., Mountain, M., Nehrkorn, T., Montzka, S. A., McKain, K., Kofler, J., Trudeau, M., Michel, S. E., Biraud, S. C., Fischer, M. L., Worthy, D.

E. J., … Van Der Velde, I. R. (2019). Enhanced North American carbon uptake associated with El Niño. *Science Advances*, *5*(6), 1–11. https://doi.org/10.1126/sciadv.aaw0076

Jeong, S.-J., Bloom, A. A., Schimel, D., Sweeney, C., Parazoo, N. C., Medvigy, D., Schaepman-Strub, G., Zheng, C., Schwalm, C. R., Huntzinger, D. N., Michalak, A. M., & Miller, C. E. (2018). Accelerating rates of Arctic carbon cycling revealed by long-term atmospheric CO_2 measurements. *Science Advances*, *4*(7), eaao1167. https://doi.org/10.1126/sciadv.aao1167

Joiner, J., Guanter, L., Lindstrot, R., Voigt, M., Vasilkov, A. P., Middleton, E. M., Huemmrich, K. F., Yoshida, Y., & Frankenberg, C. (2013). Global monitoring of terrestrial chlorophyll fluorescence from moderate-spectral-resolution near-infrared satellite measurements: methodology, simulations, and application to GOME-2. *Atmospheric Measurement Techniques*, *6*(10), 2803–2823. https://doi.org/10.5194/amt-6-2803-2013

Keenan, T. F., Gray, J., Friedl, M. A., Toomey, M., Bohrer, G., Hollinger, D. Y., Munger, J. W., O'Keefe, J., Schmid, H. P., Wing, I. S., Yang, B., & Richardson, A. D. (2014). Net carbon uptake has increased through warming-induced changes in temperate forest phenology. *Nature Climate Change*, *4*(7), 598–604. https://doi.org/10.1038/nclimate2253

Kim, J.-S., Kug, J.-S., & Jeong, S.-J. (2017). Intensification of terrestrial carbon cycle related to El Niño–Southern Oscillation under greenhouse warming. *Nature Communications*, *8*(1), 1674. https://doi.org/10.1038/s41467-017-01831-7

Le Quéré, C., Andrew, R. M., Friedlingstein, P., Sitch, S., Pongratz, J., Manning, A. C., Korsbakken, J. I., Peters, G. P., Canadell, J. G., Jackson, R. B., Boden, T. A., Tans, P. P., Andrews, O. D., Arora, V. K., Bakker, D. C. E., Barbero, L., Becker, M., Betts, R. A., Bopp, L., … Zhu, D. (2018). Global Carbon Budget 2017. *Earth System Science Data*, *10*(1), 405–448. https://doi.org/10.5194/essd-10-405-2018

Lian, X., Piao, S., Li, L. Z. X., Li, Y., Huntingford, C., Ciais, P., Cescatti, A., Janssens, I. A., Peñuelas, J., Buermann, W., Chen, A., Li, X., Myneni, R. B., Wang, X., Wang, Y., Yang, Y., Zeng, Z., Zhang, Y., & McVicar, T. R. (2020). Summer soil drying exacerbated by earlier spring greening of northern vegetation. *Science Advances*, *6*(1), eaax0255.

https://doi.org/10.1126/sciadv.aax0255

Liu, J., Bowman, K. W., Schimel, D. S., Parazoo, N. C., Jiang, Z., Lee, M., Bloom, A. A., Wunch, D., Frankenberg, C., Sun, Y., O'Dell, C. W., Gurney, K. R., Menemenlis, D., Gierach, M., Crisp, D., & Eldering, A. (2017). Contrasting carbon cycle responses of the tropical continents to the 2015–2016 El Niño. *Science*, *358*(6360), eaam5690. https://doi.org/10.1126/science.aam5690

Malhi, Y., Rowland, L., Aragão, L. E. O. C., & Fisher, R. A. (2018). New insights into the variability of the tropical land carbon cycle from the El Niño of 2015/2016. *Philosophical Transactions of the Royal Society B: Biological Sciences*, *373*(1760), 20170298. https://doi.org/10.1098/rstb.2017.0298

McPhaden, M. J., Zebiak, S. E., & Glantz, M. H. (2006). ENSO as an integrating concept in earth science. *Science*, *314*(5806), 1740–1745. https://doi.org/10.1126/science.1132588

Mystakidis, S., Seneviratne, S. I., Gruber, N., & Davin, E. L. (2017). Hydrological and biogeochemical constraints on terrestrial carbon cycle feedbacks. *Environmental Research Letters*, *12*(1), 014009. https://doi.org/10.1088/1748-9326/12/1/014009

Piao, S., Liu, Z., Wang, Y., Ciais, P., Yao, Y., Peng, S., Chevallier, F., Friedlingstein, P., Janssens, I. A., Peñuelas, J., Sitch, S., & Wang, T. (2018). On the causes of trends in the seasonal amplitude of atmospheric CO_2. *Global Change Biology*, *24*(2), 608–616. https://doi.org/10.1111/gcb.13909

Piao, S., Wang, X., Wang, K., Li, X., Bastos, A., Canadell, J. G., Ciais, P., Friedlingstein, P., & Sitch, S. (2020). Interannual variation of terrestrial carbon cycle: Issues and perspectives. *Global Change Biology*, *26*(1), 300–318. https://doi.org/10.1111/gcb.14884

Pinzon, J. E., & Tucker, C. J. (2014). A non-stationary 1981-2012 AVHRR NDVI3g time series. *Remote Sensing*, *6*(8), 6929–6960. https://doi.org/10.3390/rs6086929

Randerson, J. T., Field, C. B., Fung, I. Y., & Tans, P. P. (1999). Increases in early season ecosystem uptake explain recent changes in the seasonal cycle of atmospheric CO_2 at high northern latitudes. *Geophysical Research Letters*, *26*(17), 2765–2768. https://doi.org/10.1029/1999GL900500

Rödenbeck, C., Houweling, S., Gloor, M., & Heimann, M. (2003). CO_2 flux history 1982-2001 inferred from atmospheric data using a global inversion of atmospheric transport. *Atmospheric Chemistry and Physics*, *3*(6), 1919–1964. https://doi.org/10.5194/acp-3-1919-2003

Santoso, A., Mcphaden, M. J., & Cai, W. (2017). The Defining Characteristics of ENSO Extremes and the Strong 2015/2016 El Niño. *Reviews of Geophysics*, *55*(4), 1079–1129. https://doi.org/10.1002/2017RG000560

Scripps Institution of Oceanography. (2020). *The Keeling Curve*. https://scripps.ucsd.edu/programs/keelingcurve/

Sitch, S., Friedlingstein, P., Gruber, N., Jones, S. D., Murray-Tortarolo, G., Ahlström, A., Doney, S. C., Graven, H., Heinze, C., Huntingford, C., Levis, S., Levy, P. E., Lomas, M., Poulter, B., Viovy, N., Zaehle, S., Zeng, N., Arneth, A., Bonan, G., … Myneni, R. (2015). Recent trends and drivers of regional sources and sinks of carbon dioxide. *Biogeosciences*, *12*(3), 653–679. https://doi.org/10.5194/bg-12-653-2015

Thoning, K. W., Tans, P. P., & Komhyr, W. D. (1989). Atmospheric carbon dioxide at Mauna Loa Observatory: 2. Analysis of the NOAA GMCC data, 1974-1985. *Journal of Geophysical Research: Atmospheres*, *94*(D6), 8549–8565. https://doi.org/10.1029/JD094iD06p08549

Timmermann, A., An, S., Kug, J., Jin, F., Cai, W., Capotondi, A., Cobb, K. M., Lengaigne, M., McPhaden, M. J., Stuecker, M. F., Stein, K., Wittenberg, A. T., Yun, K., Bayr, T., Chen, H., Chikamoto, Y., Dewitte, B., Dommenget, D., Grothe, P., … Zhang, X. (2018). El Niño–Southern Oscillation complexity. *Nature*, *559*(7715), 535–545. https://doi.org/10.1038/s41586-018-0252-6

Wang, B., Luo, X., Yang, Y. M., Sun, W., Cane, M. A., Cai, W., Yeh, S. W., & Liu, J. (2019). Historical change of El Niño properties sheds light on future changes of extreme El Niño. *Proceedings of the National Academy of Sciences of the United States of America*, *116*(45), 22512–22517. https://doi.org/10.1073/pnas.1911130116

Wang, J., Zeng, N., Wang, M., Jiang, F., Wang, H., & Jiang, Z. (2018). Contrasting terrestrial carbon cycle responses to the 1997/98 and 2015/16 extreme El Niño events. *Earth System*

Dynamics, *9*(1), 1–14. https://doi.org/10.5194/esd-9-1-2018

Wang, K., Wang, Y., Wang, X., He, Y., Li, X., Keeling, R. F., Ciais, P., Heimann, M., Peng, S., Chevallier, F., Friedlingstein, P., Sitch, S., Buermann, W., Arora, V. K., Haverd, V., Jain, A. K., Kato, E., Lienert, S., Lombardozzi, D., … Piao, S. (2020). Causes of slowing-down seasonal CO_2 amplitude at Mauna Loa. *Global Change Biology*, *26*(8), 4462–4477. https://doi.org/10.1111/gcb.15162

Wang, W., Ciais, P., Nemani, R. R., Canadell, J. G., Piao, S., Sitch, S., White, M. A., Hashimoto, H., Milesi, C., & Myneni, R. B. (2013). Variations in atmospheric CO_2 growth rates coupled with tropical temperature. *Proceedings of the National Academy of Sciences*, *110*(32), 13061–13066. https://doi.org/10.1073/pnas.1219683110

Yue, C., Ciais, P., Bastos, A., Chevallier, F., Yin, Y., Rödenbeck, C., & Park, T. (2017). Vegetation greenness and land carbon-flux anomalies associated with climate variations: A focus on the year 2015. *Atmospheric Chemistry and Physics*, *17*(22), 13903–13919. https://doi.org/10.5194/acp-17-13903-2017

Zhang, Y., Commane, R., Zhou, S., Williams, A. P., & Gentine, P. (2020). Light limitation regulates the response of autumn terrestrial carbon uptake to warming. *Nature Climate Change*, *10*(8), 739–743. https://doi.org/10.1038/s41558-020-0806-0

ACKNOWLEDGEMENTS

We thank Dr. Pieter Tans and Dr. Ed Dlugokencky for providing the CO_2 mole fraction data. We also thank the TRENDYv6 modelers for their simulations and Dr. Christian Rödenbeck for the Jena CarboScope inversion datasets. This study was supported by the Strategic Priority Research Program (A) of the Chinese Academy of Sciences (grant XDA20050101), Second Tibetan Plateau Scientific Expedition and Research Program (2019QZKK0208), National Natural Science Foundation of China (41861134036 and 41988101), and an Oak Ridge National Lab subcontract (4000167205). J. Mao and X. Shi were supported by the Reducing Uncertainties in Biogeochemical Interactions through Synthesis and Computation Science Focus Area and the Terrestrial Ecosystem Science Scientific Focus Area project in the Earth and Environmental Systems Sciences Division of the Biological and Environmental Research (BER) office in the US Department of Energy Office of Science. Oak Ridge National Laboratory is supported by the Office of Science of the US Department of Energy under Contract No. DE-AC05-00OR22725.

DATA AVAILABILITY STATEMENT

Monthly CO_2 mole fraction data from the NOAA ESRL Carbon Cycle Cooperative Global Air Sampling Network is available at ftp://aftp.cmdl.noaa.gov/data/trace_gases/co2/flask/. Monthly gridded air temperature and precipitation data from the Climatic Research Unit are available at https://crudata.uea.ac.uk/cru/data/hrg/. Satellite SIF datasets are retrieved from https://avdc.gsfc.nasa.gov/pub/data/satellite/MetOp/GOME_F/. Jena CarboScope datasets are available at http://www.bgc-jena.mpg.de/CarboScope/. The TRENDYv6 data are available from Stephen Sitch (s.a.sitch@exeter.ac.uk) or Pierre Friedlingstein (p.friedlingstein@exeter.ac.uk) upon reasonable request. All the relevant data from this study are also available from the corresponding author upon request.

CONFLICT OF INTEREST STATEMENT

The authors declare no conflict of interest.

Figure Captions:

FIGURE 1 Unusual atmospheric CO_2 growth rate (CGR) and CO_2 seasonal-cycle amplitude (SCA) at Mauna Loa (MLO) in 2015−2016. (a) The relationship between detrended CGR anomaly and SCA anomaly at MLO during El Niño events since 1980. (b) SCA anomalies at 32 atmospheric observation sites in the average ("Composite") of El Niño events and in 2015−2016 El Niño, shown as a histogram for all locations, and by the latitudes of the individual observation sites. (c) The relationship between SCA anomaly at MLO and annual net biome productivity (NBP) anomaly in northern extra-tropics (north of 30°N), and during El Niño occurrences. (d) The relationship between tropical (30°S−30°N) annual NBP anomaly and CGR anomaly at MLO, in El Niño years. NBP anomaly is estimated by two atmospheric inversions, CAMS and Jena CarboScope. In panels a, c and d, the dashed lines indicate the 95% confidence interval for the regression fit (see also annotations for regression statistics). In panel b, solid lines indicate the inter-quartile range of SCA anomaly during El Niño events and two asterisks indicate that overall, the SCA in 2015−2016 is significantly larger than SCA "Composite" values. Grey lines in panels c and d indicate the range of NBP anomaly, from atmospheric inversions, for each El Niño event

FIGURE 2 Monthly NBP anomaly in the northern extra-tropics during 2015−2016. NBP anomaly is estimated by two atmospheric in situ data-based inversions (CAMS and Jena CarboScope) (a) and an ensemble of DGVMs (b). Black lines indicate the mean NBP anomaly of ten El Niño events since 1980 ("Composite") while red lines indicate the mean NBP anomaly for 2015 and 2016, which are estimated by the average of inversions (a) or DGVMs (b). The spread each side of the solid lines are the range of inversions (a) or 1-σ inter-model spread (b). Positive anomalies of NBP mainly occurred in April−June of 2015−2016 (blue shaded area) and negative anomalies of NBP are mainly occurred in August−September of 2015−2016 (yellow shaded area). The zero anomaly line is shown in both panels as a dotted line

FIGURE 3 Normalized NBP anomalies during April−June and August−September of 2015−2016. NBP anomaly is estimated by the $CAMS_{OCO\text{-}2}$ inversion inferred from the OCO-2 X_{co2} retrievals (a, b), two atmospheric in situ inversions CAMS (c, d) and Jena CarboScope (e, f), and an ensemble of TRENDY DGVMs (g, h). In panels g and h, only gridded pixels where the signs of

NBP anomaly derived from more than 8 of 12 models are consistent with those from the average of DGVMs are shown. In each panel, the NBP anomaly is normalized by the spatial standard deviation of the NBP anomaly for clarity

FIGURE 4 Vegetation productivity anomalies during April−June and August−September of 2015−2016. Vegetation productivity is estimated from vegetation greenness (NDVI) (a, b), sun-induced chlorophyll fluorescence (SIF) (c, d) and modeled gross primary productivity (GPP) of DGVMs (e, f). In panels e and f, only gridded pixels where the signs of NBP anomaly derived from more than 8 of 12 models are consistent with those from the average of DGVMs are shown

FIGURE 5 Anomalies of monthly carbon fluxes and monthly climatic drivers in 2015−2016. Vegetation productivity (NDVI, SIF and modeled GPP) (top row), respiration fluxes (Ra and Rh) (middle row) and climatic drivers (bottom row) are estimated in two regions of western North America and western Russia where each grid cell has higher spring net carbon uptake during 2015−2016 than the long-term average. Climatic drivers include temperature (T), precipitation (P) and shortwave radiation (Rad). All variables in each month are normalized by their standard deviation during 1980−2016 ("z-score"). Shaded area indicates the uncertainties for the extents of the two regions, which are based on different DGVM estimations imposed on them

FIGURE 6 Schematic of the effect of earlier greening in spring on the net carbon sink in early autumn of 2015−2016. Higher spring temperature causes the earlier greening and thus stronger productivity in spring. Stronger productivity leads to more evapotranspiration (ET) and the decrease of soil water content (SWC). The carryover of soil moisture could weaken the productivity (GPP) in the following seasons, including autumn. Enhanced productivity in spring also allows more carbon into the litter pool, that could increase the heterotrophic respiration (Rh) in early autumn. Both weakened GPP and strengthened Rh would cause the decrease of net biome productivity (NBP)

Figure 1

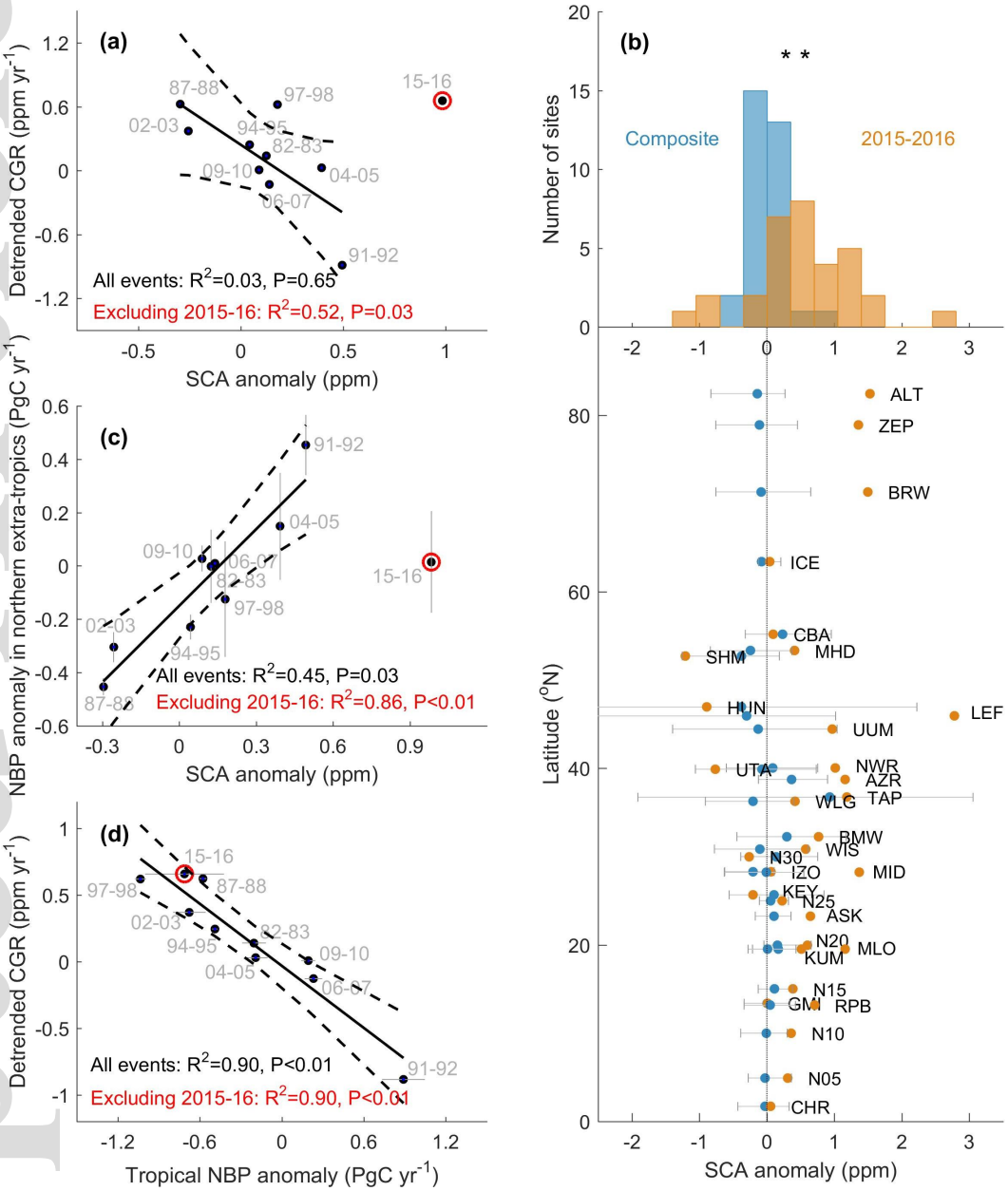

Figure 2

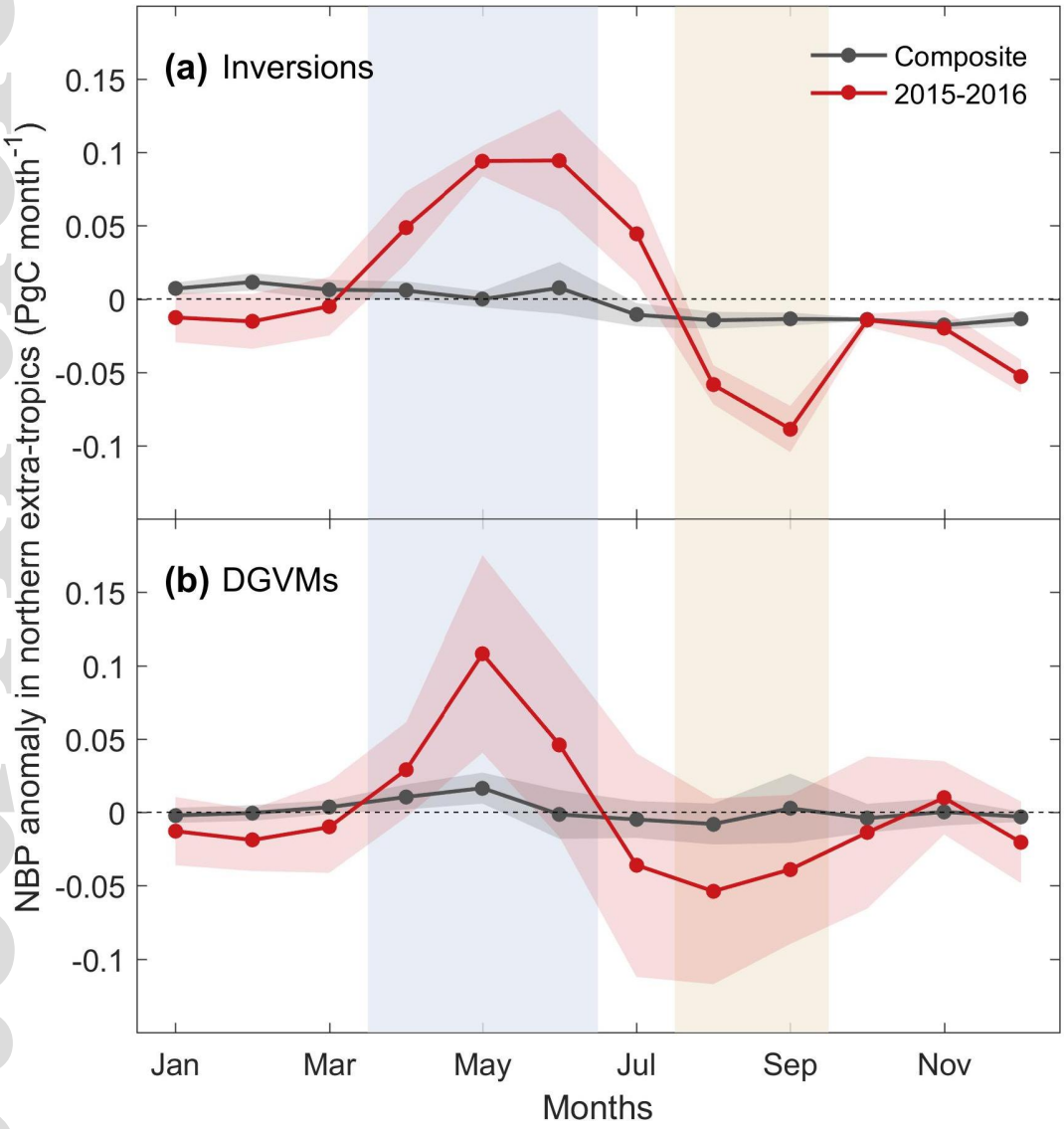

Figure 3

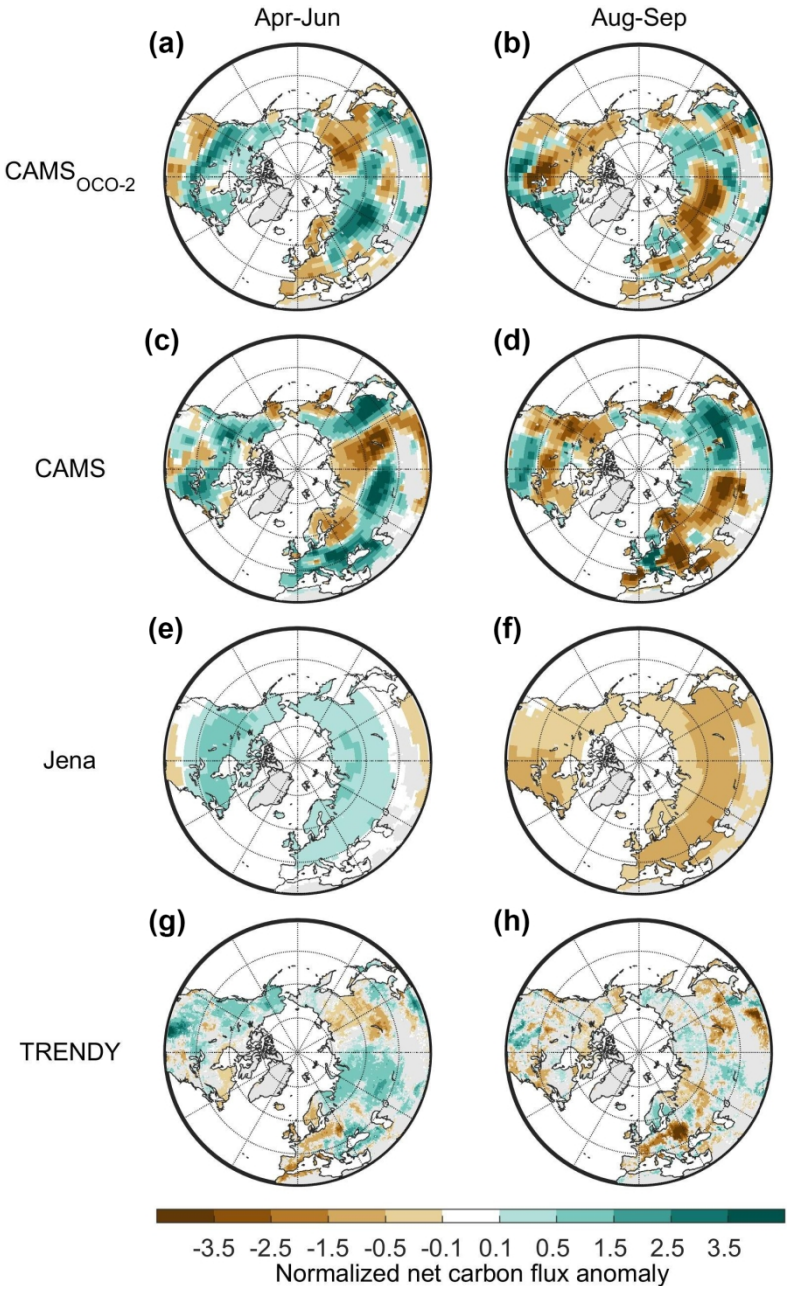

Figure 4

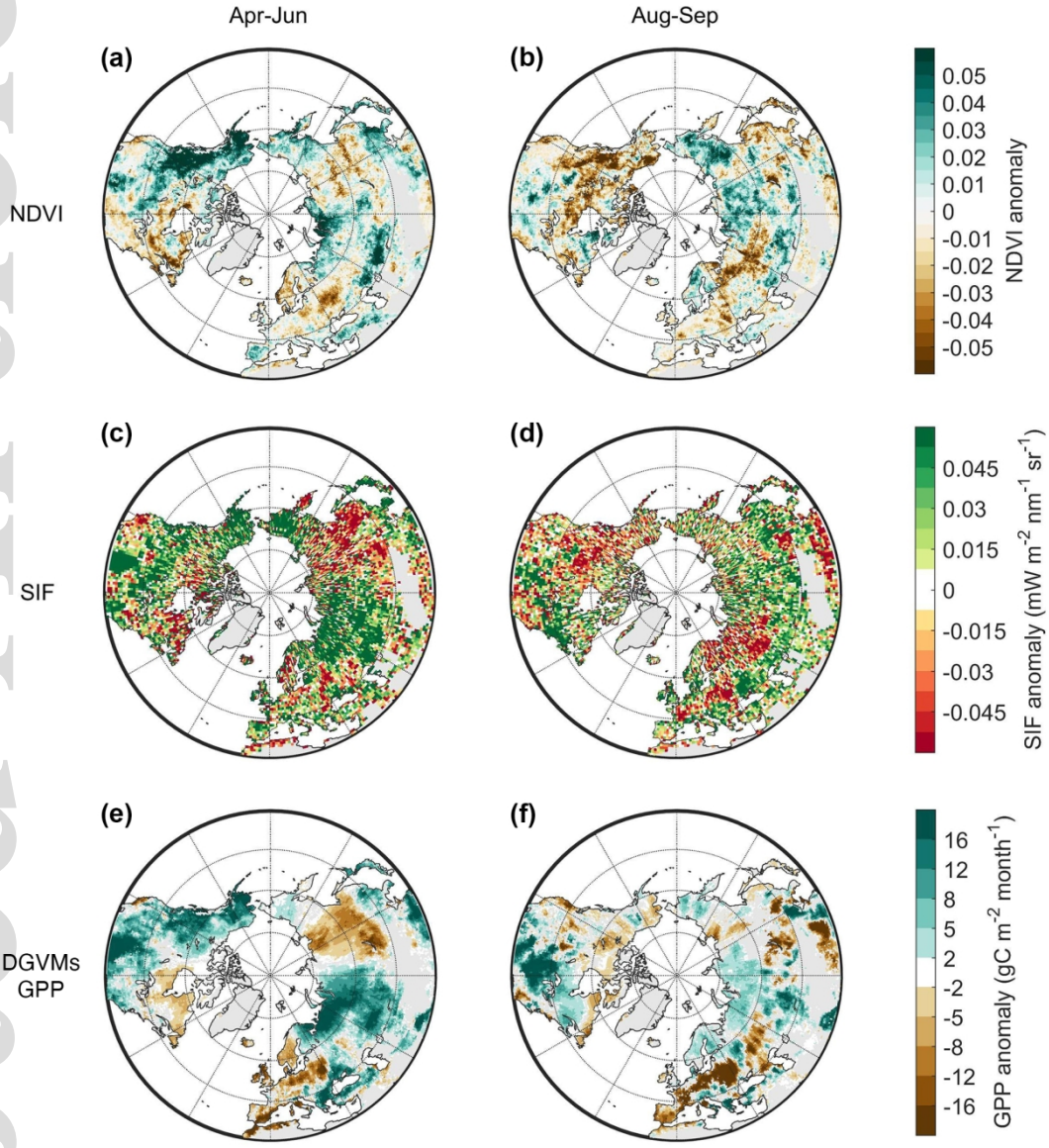

Figure 5

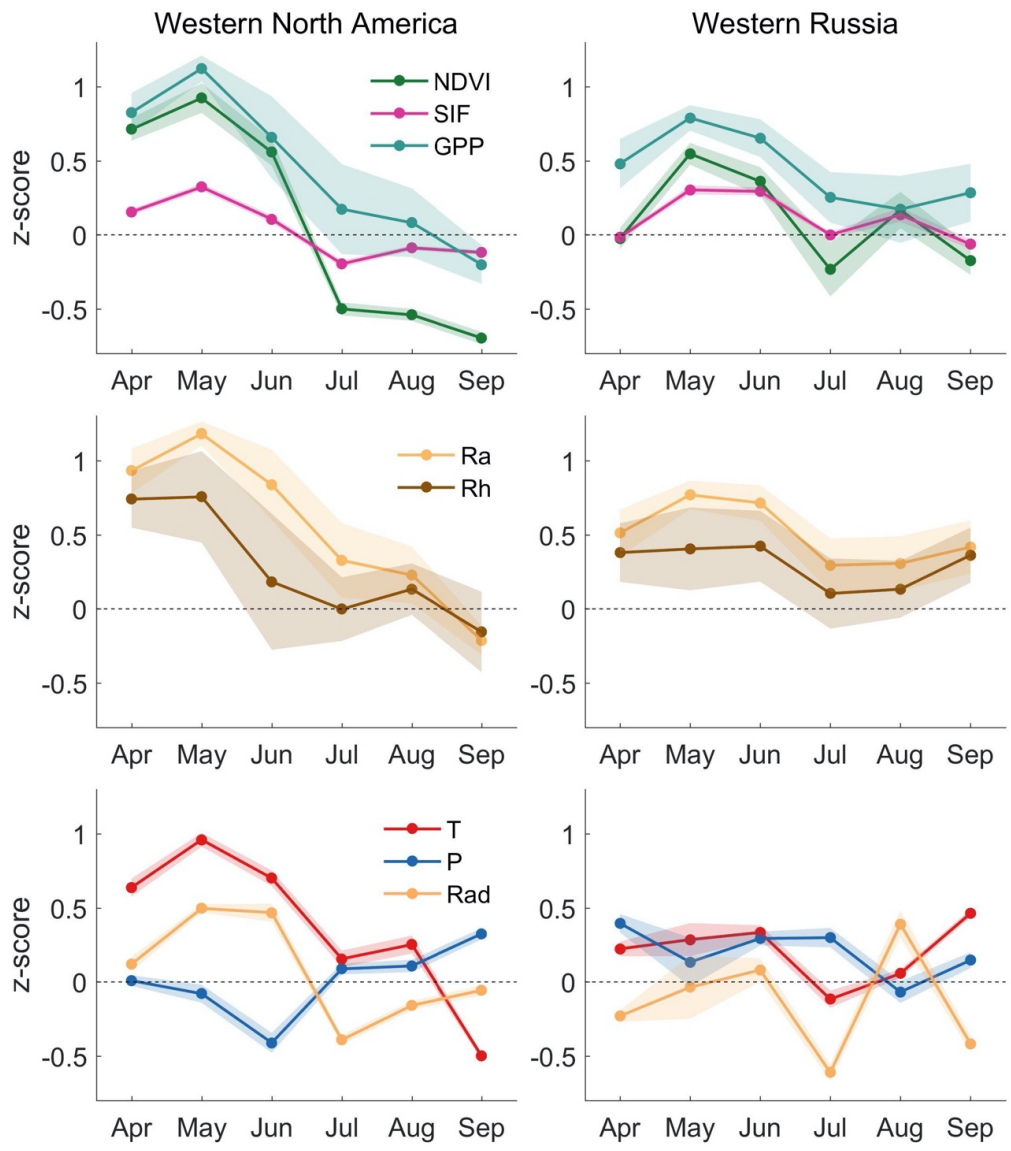

Figure 6